

Optimization in Tri-axial Degaussing System Design and Estimation of Degaussing Coil Currents

Vishal Modagekar, Shaikh Abdul Karim, Navdeep Singh, and Faruk Kazi

Department of Electrical Engineering, Veermata Jijabai Technological Institute, Matunga, Mumbai 400019, India

Contemporary ships, made of ferromagnetic materials, under the influence of Earth's magnetic field produce an underwater magnetic anomaly. This anomaly, often called the magnetic signature, compromises the stealth and safety of the ship and needs to be minimized. This paper presents an efficient methodology for the design of optimal tri-axial degaussing system and estimation of coil currents in ships to minimize the magnetic signature of the ship. Designing such a system is a complex optimization problem, we address this problem with high dimensional variable selection technique along with linear regression techniques.

Index Terms—Degaussing, magnetic signatures, optimization, least angle regression (LARS), tilted correlation screening (TCS), ridge regression.

I. INTRODUCTION

SHIPS made of ferromagnetic materials interact with the ambient magnetic field thus creating a magnetic anomaly in the region of their presence, which makes them susceptible to magnetic influence mines that are triggered on sensing the underwater magnetic anomaly. To minimize this magnetic signature and to maintain stealth and safety, degaussing coils are used in modern ships. Since the Earth's magnetic field can be expressed in three orthogonal components, degaussing coils are present in all these three directions to counter the anomaly due to each individual component effectively [1],[2].

Simulation softwares based on finite element numerical techniques are typically used for detailed modeling of ferromagnetic signatures of ships and submarines [3], here we have used COBHAM Opera3D for these simulations. Reference [4] proposes the application of least angle regression (LARS) [5] in designing a degaussing system, wherein a large number of coils than that are actually being placed are considered, and then LARS is applied on the signature and the coil effects data that is extracted from simulation, to rank the coils according to their contribution in reducing the signature. This algorithm runs in a iterative manner, wherein each iteration a new variable (coil) is added to form a model to best approximate the signature. The algorithm also provides currents in the selected coils, such that the residual magnetic signature is as small as possible for each model formed iteratively. The underlying assumption for applying such technique is that the magnetic signature of a ship can be approximated by energizing finite number of coils placed strategically inside it. Also even if the material used in ship is ferromagnetic in nature, the permeability is approximately constant under the operating conditions. Thus the application of variable selection and linear regression model formulation techniques is justified. However, LARS is susceptible to high correlation among the predictors and thus give spurious inferences. The

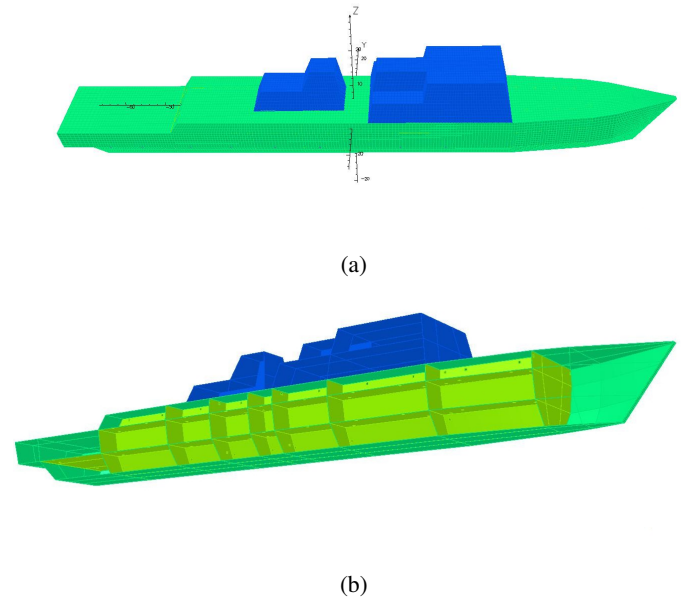


Fig. 1: Ship model. (a) External view with coordinate axes. (b) Section view showing internal decks and bulkheads.

failure of LARS is attributed towards its variable selection procedure that is based on marginal correlation [5].

To make the variable selection and model formulation procedure robust we show that tilted correlation screening along with generalized ridge regression (TCS-GRR) can be a feasible option. We demonstrate the same by comparing the results and inferences obtained by applying both LARS and TCS-GRR techniques on the aforementioned degaussing problem. We also show that such a methodology not only ranks the coils, but also helps in designing new coils apart from the initially considered set of coils.

II. DESIGNING THE DEGAUSSING COILS

In order to evaluate the induced magnetization by Earth's magnetic field a ship is modeled in Opera3D. The ship model incorporates elements like decks, internal bulkheads and superstructure. Fig. 1 shows the model of the ship with right handed coordinate system on it and the section view depicting

Manuscript received September 15, 2016; revised November 11, 2016; accepted December 17, 2016. Corresponding author: V. Modagekar (email: vcmodagekar@gmail.com).

Digital Object Identifier 10.1109/TMAG.2016.2642890

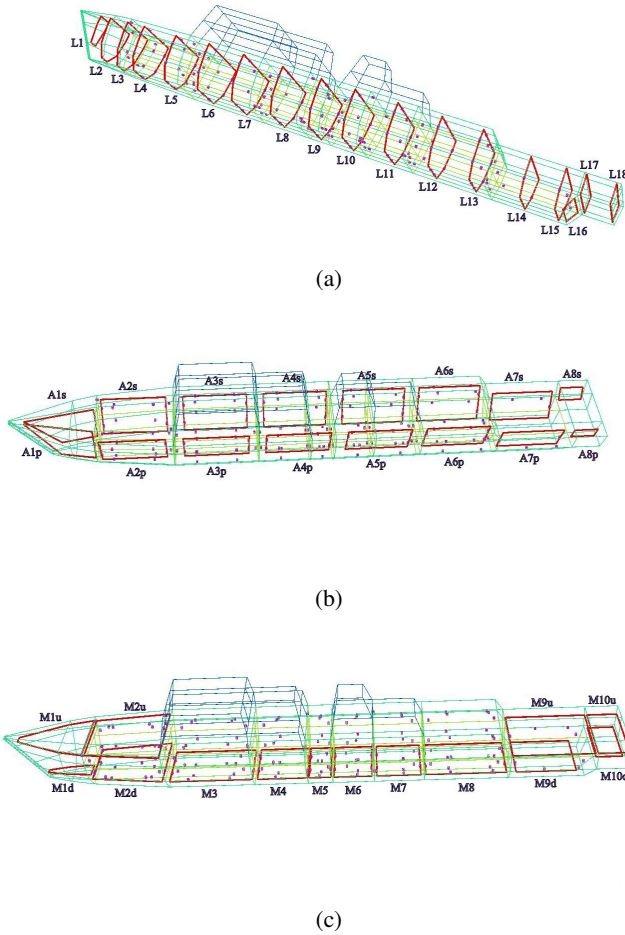


Fig. 2: Tri-axial degaussing coils. (a) Longitudinal coils. (b) Athwartship coils. (c) Vertical or main coils.

the internal structure. The modeled ship has the following dimensions: length = 150 m, width = 20 m and height = 12 m. The superstructure is assigned with a BH curve of material that is magnetically weak as compared to the remaining part of the model.

Traditional ship degaussing systems consists of coil sets that are designed to be orthogonal to the field components (B_x, B_y, B_z) with respect to ship reference frame [2]. Since mine sensitivity has improved in all the three directions [1], need arises for more complex coil designs to reduce the magnetic signature to significant levels. Originally, we used the traditional degaussing coil design as in [2], but after careful considerations aided by the proposed algorithm we have modified the designs as shown in Fig. 2. The athwartship coils in the midsection are tilted with respect to the vertical plane passing through the keel line of the ship, rather than being orthogonal to the Y-axis as implemented by [6], such coils proved to be more effective in reducing the magnetic field components of ship in both Y- and Z-direction. The A-coils in the bow region, namely A1p and A1s have been specifically designed by us such that they lie in the plane parallel to the side planks joined at the stem. This unconventional coil design effectively reduces the magnetic field components in both X- and Y-direction, so much so that the L-coils, namely L1 and L2 can be omitted. Again, coil

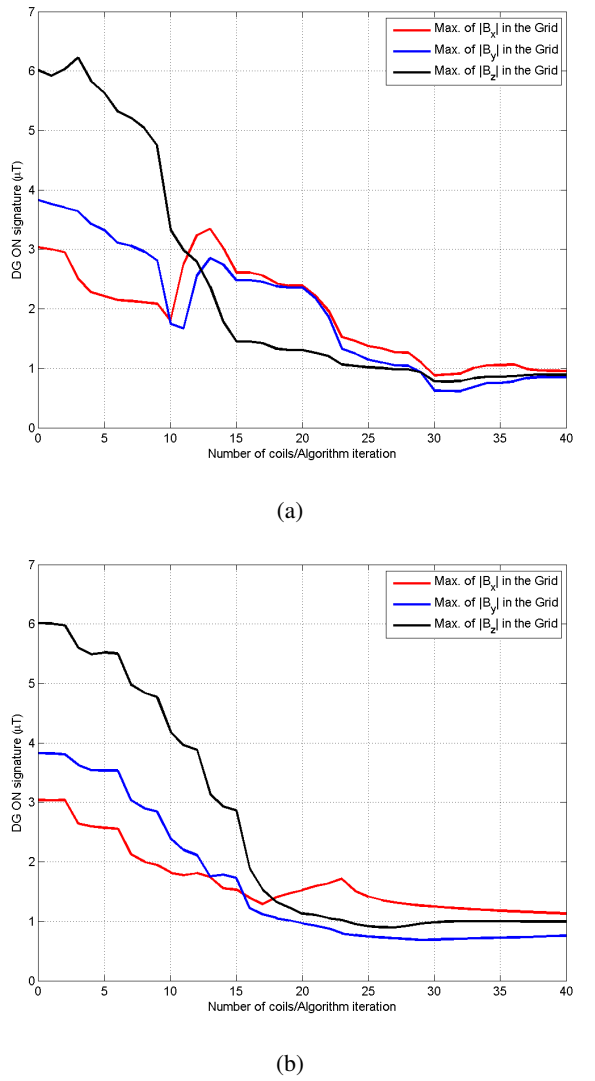


Fig. 3: Calculated DG ON signature reduction trend in the measurement grid for external field $50 \mu\text{T}$ in Z-direction. (a) LARS. (b) TCS-GRR.

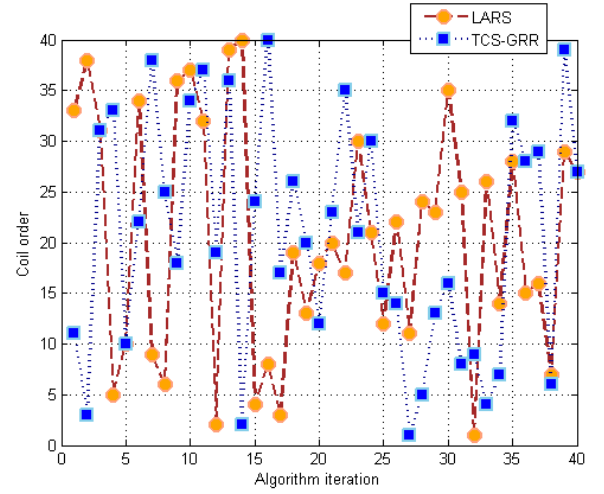
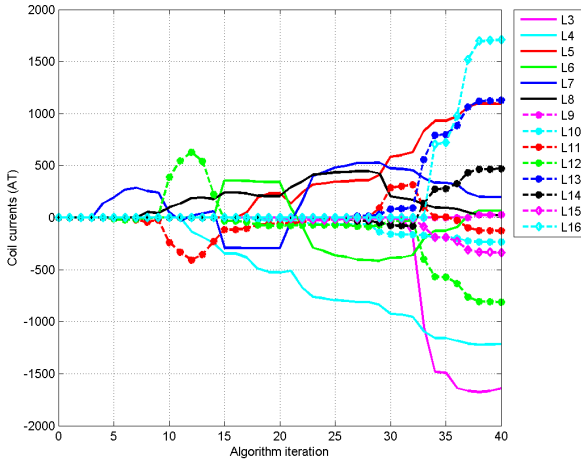
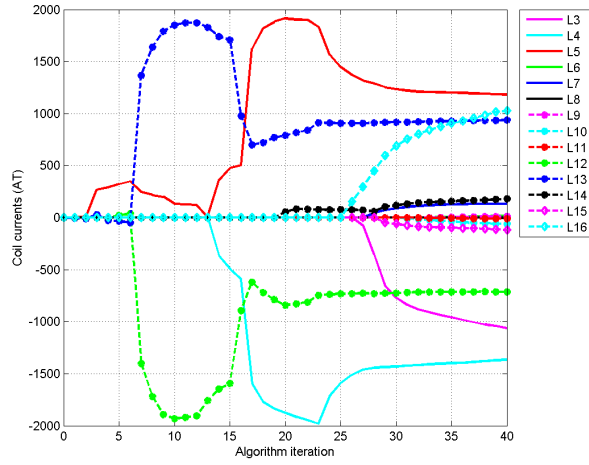


Fig. 4: Selection of coils as the respective algorithm proceeds.

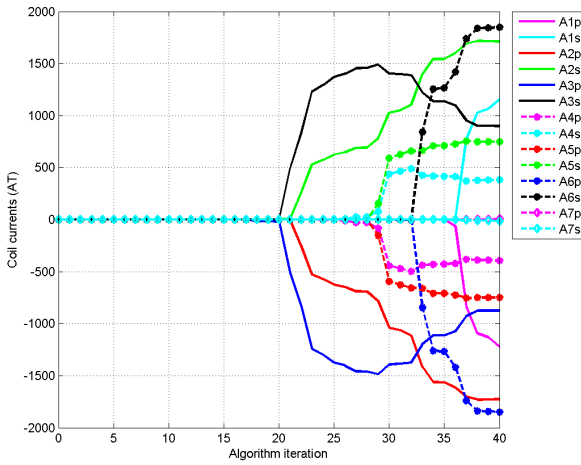
L16 has been specifically designed by us to be more effective in its ambience, it is quite different than the rest of L-coils, that it avoids the use of M10d and M10u totally. We also



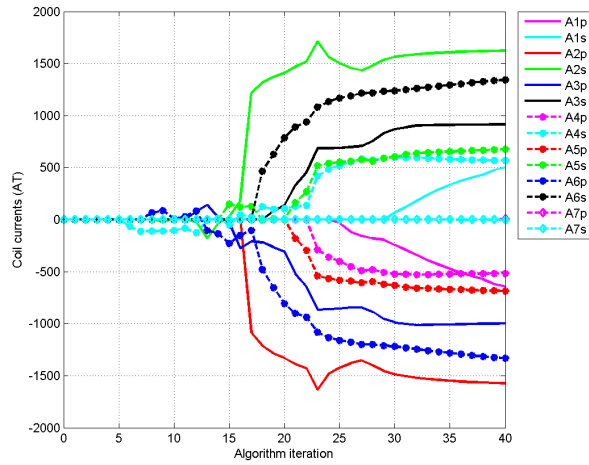
(a)



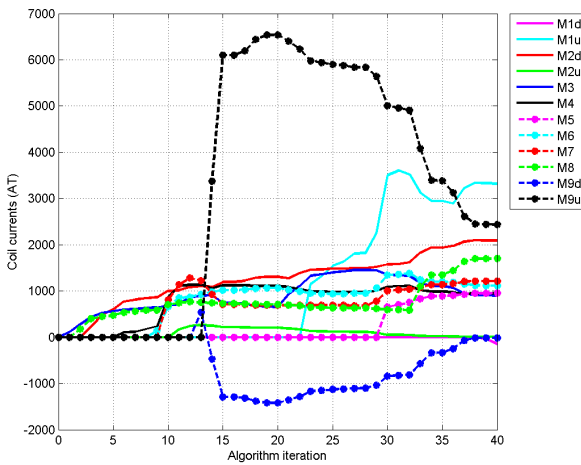
(a)



(b)



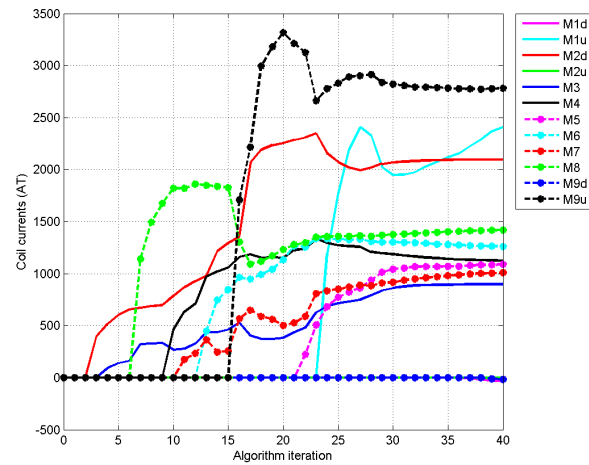
(b)



(c)

Fig. 5: The degaussing coil currents assigned by LARS for external field $50 \mu T$ in Z-direction. (a) L-coils. (b) A-coils. (c) M-coils.

noticed that inclusion of coils L17, L18, A8p and A8s does not contribute much to signature reduction. In section V we provide insights regarding how we designed coil L16 and on



(c)

Fig. 6: The degaussing coil currents assigned by TCS-GRR for external field $50 \mu T$ in Z-direction. (a) L-coils. (b) A-coils. (c) M-coils.

omission of the aforementioned 6 coils at the rear end of the ship. Thus, we finally have total 40 coils to work with, that is, 14 L-coils that are in longitudinal direction, 14 A-coils in the

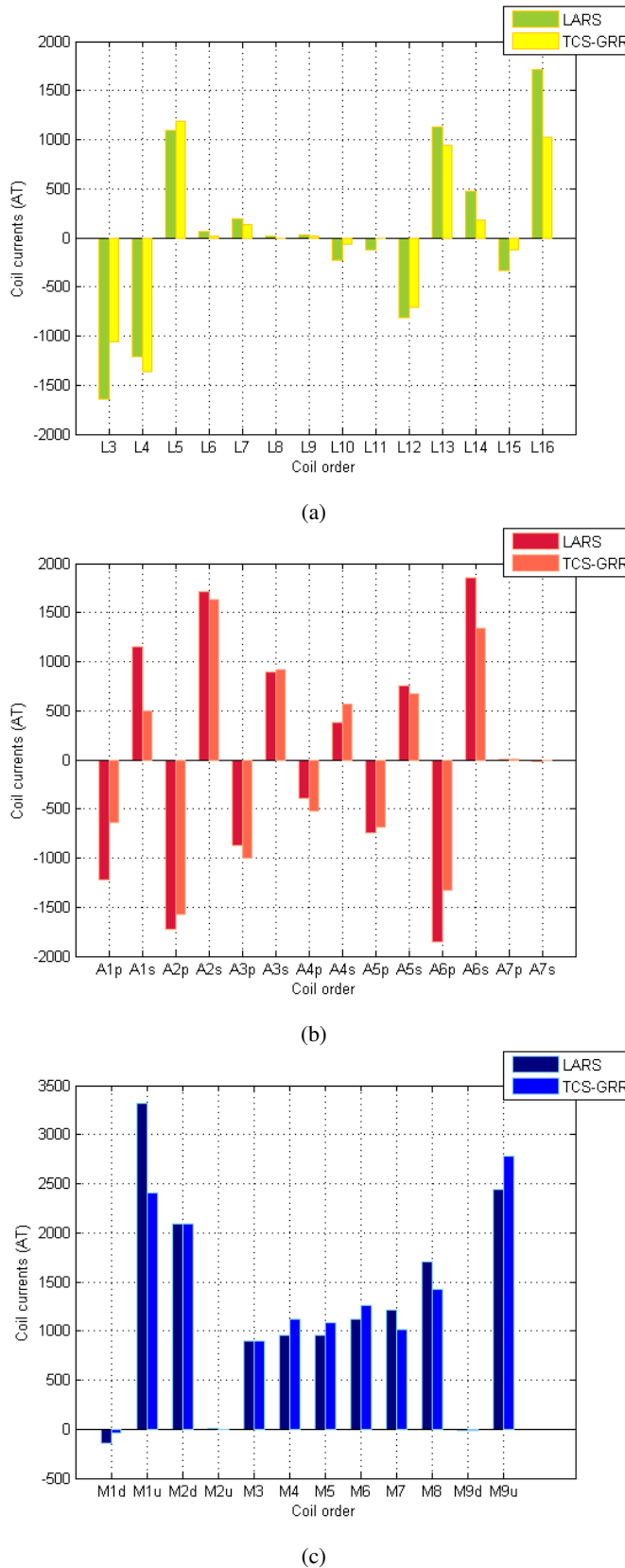


Fig. 7: Final coil currents obtained by the algorithms. (a) L-coils. (b) A-coils. (c) M-coils.

athwartship direction and 12 M-coils in the vertical direction (all directions are in ship reference frame).

The aim of incorporating the degaussing coils is to generate

magnetic field that is equal in shape and magnitude to the uncompensated signature, but in opposite direction. This artificially generated field, to compensate the signature is formed by linear combination of the fields by the individual coils. Thus, the given distribution of coils is optimal, if it generates the signature in opposite direction as close as possible to the uncompensated signature with minimum number of coils while maintaining a constraint on the maximum magnitude of current in each of the coils.

III. PROBLEM MODELING

Consider the problem of estimating a p -vector of parameters β from the linear model

$$\mathbf{y} = \mathbf{X}\beta + \epsilon,$$

where $\mathbf{y} = (y_1, \dots, y_n)^T$ is an n -vector of responses, $\mathbf{X} = (X_1, \dots, X_p)^T$ is an $(n \times p)$ design matrix and $\epsilon = (\epsilon_1, \dots, \epsilon_n)^T$ is an n -vector of independent and identically distributed random errors. When dimension p is high, it is often assumed that only a small number of predictors among X_1, \dots, X_p contribute to the response, which amounts to assuming ideally that the parameter vector β is sparse. With sparsity, variable selection can improve the accuracy of estimation by effectively identifying the subset of important predictors, and also enhance model interpretability with parsimonious representation.

In context of our problem we sampled the magnetic flux density at 1 m interval in a rectangular grid of length 200 m and width 34 m at a distance of 17 m below the keel line, symmetric with the ship model. Let N be the total number of sample points on the grid and n be the number of observations, thus $N = 7035$ and $n = 3N$, since each component (B_x, B_y, B_z) of the produced anomaly has to be taken into account at each of the N points. The response vector \mathbf{y} is composed of sampled magnetic signature (μT) measurements in the grid for some external (Earth's) field, while current in all the coils is set to zero. Thus, \mathbf{y} is a column vector having 21105 elements. To find the coil effects we sampled the simulated magnetic field, with zero external inducing field, for a reference MMF of 100 ampere-turns (AT) in each coil individually and then divided by 100, to get the measurements in tesla/ampere-turns. Each column of the design matrix \mathbf{X} represent the individual coil effects in $\mu T/AT$ for p number of coils and n observations. Thus, dimension of matrix \mathbf{X} is (21105×40) . The negative of the vector β gives the currents in ampere-turns to reduce the magnetic signature given by the response vector \mathbf{y} .

The problem of multi-collinearity in this context arises when the measurements are taken for identical or symmetrical coils that are placed in close proximity to each other, or the measurement grid is very distant to the keel line of the ship.

IV. AUTOMATED MODEL BUILDING ALGORITHM

The LARS algorithm is a less greedy forward model selection procedure. At the beginning of LARS, a predictor enters the model if its absolute marginal correlation with the response is the largest among all the predictors. The coefficient of this predictor grows in its ordinary least square

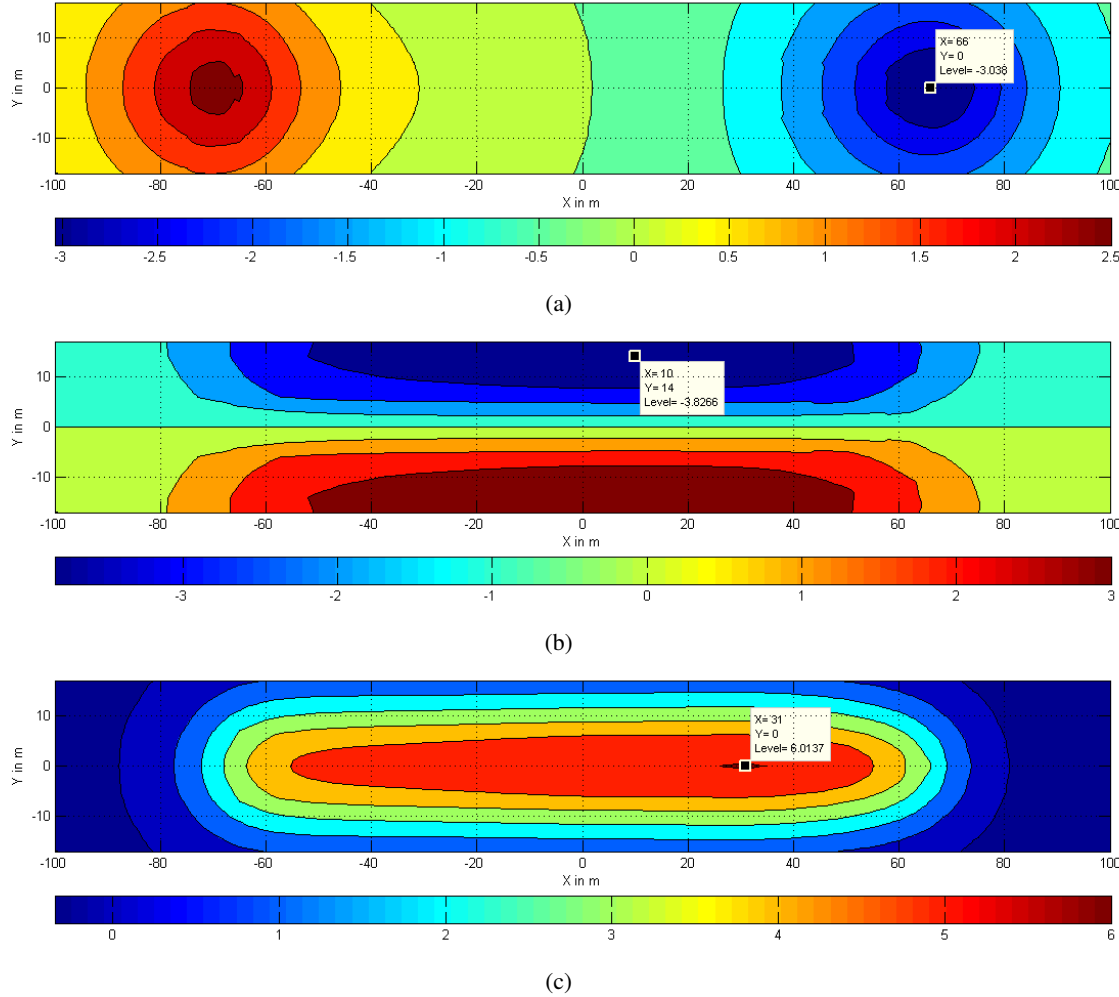


Fig. 8: Sampled DG OFF signature (μT) for external inducing field $50 \mu T$ in the Z-direction in the measurement grid. (a) X-component. (b) Y-component. (c) Z-component.

TABLE I: COMPARISON OF REDUCTION IN MAGNETIC SIGNATURE BETWEEN TCS-GRR AND LARS

External inducing field (μT) B_x B_y B_z	DG OFF signature (μT)			DG ON signature by TCS-GRR (μT)			DG ON signature by LARS (μT)		
	$ B_x $	$ B_y $	$ B_z $	$ B_x $	$ B_y $	$ B_z $	$ B_x $	$ B_y $	$ B_z $
50 0 0	15.310	10.711	25.733	1.247	1.008	1.619	1.475	1.229	2.210
0 50 0	1.424	7.119	4.767	0.747	0.990	0.810	0.723	0.968	0.805
0 0 50	3.038	3.827	6.014	1.130	0.758	0.995	0.955	0.852	0.891
50 50 50	15.335	14.783	30.434	1.982	1.826	1.946	2.378	2.465	1.965
50 50 0	15.310	12.151	26.708	2.157	1.285	1.642	1.831	1.682	2.023
0 50 50	3.359	8.402	8.507	0.976	1.298	1.047	1.090	1.240	1.022
50 0 50	15.335	13.194	29.527	2.588	1.759	2.198	2.319	2.012	2.052

direction until another predictor has the same correlation with the current residual (i.e. equal-angle). Next, both coefficients of the two picked predictors begin to move along their ordinary least square directions until a third predictor has the same correlation with the current residual as the first two. The whole process continues until all the predictors enter the model. In each step, one variable adds into the model and the regularization solution paths are extended in a piecewise linear way. After all the variables enter the model, the LARS solution paths are completed.

Marginal correlation between a variable and response is generally used to quantify the level of association between them by most of the variable selection techniques. However, this measure does not account for the correlation structure among the variables. As a result the selected variables are

not the actual underlying causal variables and neither is the model formed by them. Tilted correlation reduces the impact of irrelevant variables that are correlated to the relevant ones. In tilted correlation screening (TCS) [7] at each iteration the irrelevant variables are identified adaptively by hard-thresholding the sample correlation matrix of the variables. The threshold is calculated based on controlling the false discovery rate (FDR) [8] to minimize the Type I errors.

In TCS, at each iteration the regression coefficient vector is evaluated by setting the coefficients corresponding to selected variables to be the least squares estimate and the rest to be equal to zero. Since ordinary least square often does poorly when the correlations among the variables are very high and or the noise level is high, we instead use ridge estimates. Thus, at each iteration we perform generalized ridge regression [9]

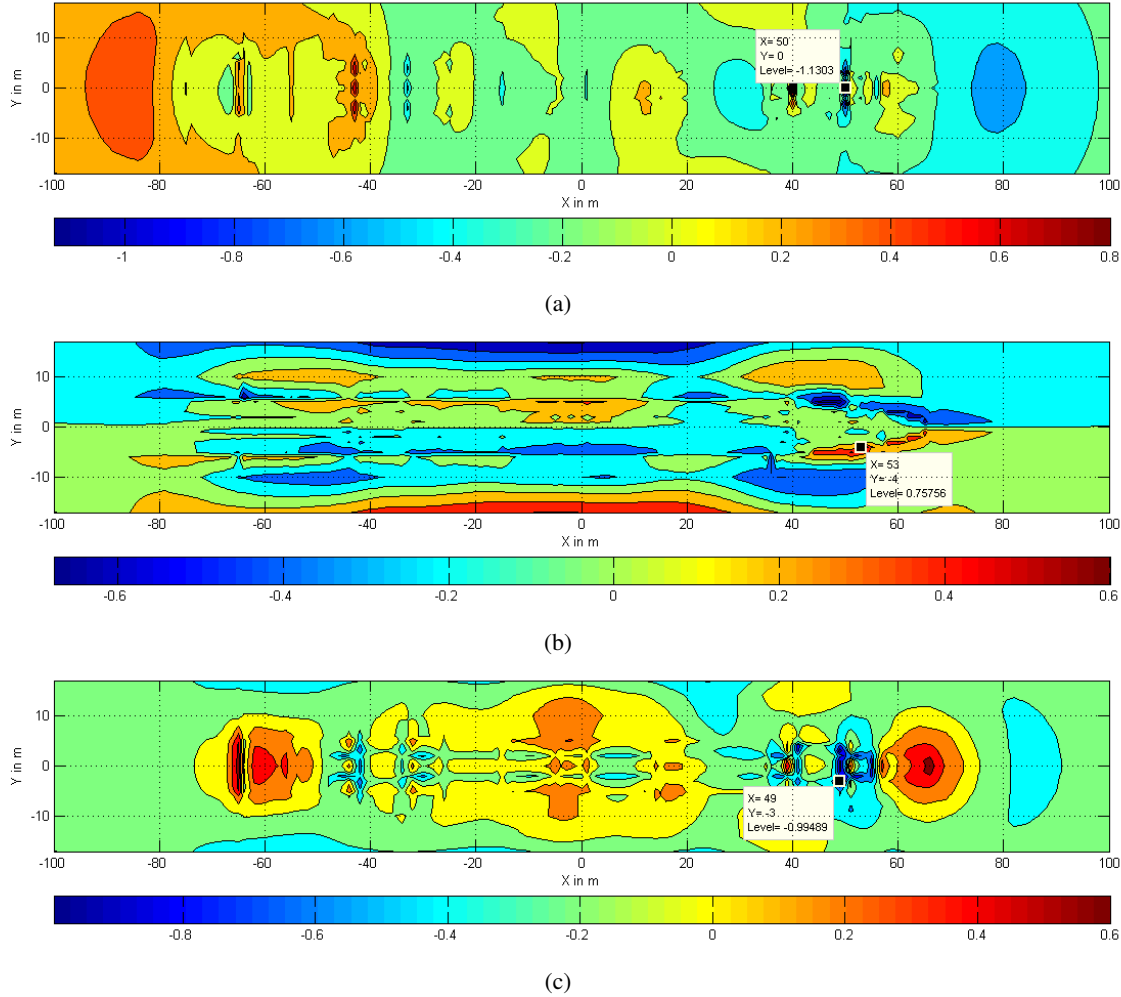


Fig. 9: Calculated DG ON signature (μT) for external inducing field $50 \mu T$ in the Z-direction in the measurement grid. (a) X-component. (b) Y-component. (c) Z-component.

on the variables in the active set and the residual response to obtain regression coefficients that have correct signs and plausible magnitudes, we call this algorithm as TCS-GRR. In ridge regression, ridge parameter plays an important role in estimation of the regression coefficients, we derive our ridge parameters from [10].

The TCS-GRR algorithm is as follows:

Step 0 Start with an empty active set \mathcal{A} , current residual $\mathbf{z} = \mathbf{y}$, current design matrix $\mathbf{Z} = \mathbf{X}$, initial regression coefficient vector $\beta_0 = 0$ and iteration count $t = 1$. \mathbf{Z} is normalized to have unit norm for each column.

Step 1 For every $j \notin \mathcal{A}$, compute the marginal correlation between \mathbf{z} and Z_j and let $m = \arg \max_{j \notin \mathcal{A}} |Z_j^T \mathbf{z}|$.

Step 2 Compute the correlation matrix $\mathbf{C} = \mathbf{Z}^T \mathbf{Z}$ and the threshold π_n based on FDR to pick the variables which have strong correlations with variable m . Find $C_m = \{j \notin \mathcal{A}, j \neq m : |c_{mj}| > \pi_n\}$, where c_{mj} is the element of matrix \mathbf{C} . If $C_m = \emptyset$, add m to \mathcal{A} and go to Step 4.

Step 3 For each $l \in C_m \cup m$, let $\tilde{\mathbf{Z}}_l = \mathbf{Z}_{C_l}$, where $C_l = \{j \notin \mathcal{A}, j \neq l : |c_{lj}| > \pi_n\}$, and compute the projection matrix $\Pi_l = \tilde{\mathbf{Z}}_l (\tilde{\mathbf{Z}}_l^T \tilde{\mathbf{Z}}_l)^{-1} \tilde{\mathbf{Z}}_l^T$. Find

$$m' = \max_{l \in C_m \cup m} |c_l^*|, \text{ where } c_l^* = s_l^{-1} ((\mathbf{I}_n - \Pi_l) \mathbf{Z}_l)^T \mathbf{z}$$

$$\text{and } s_l = 1 - a_l \text{ and } a_l = \frac{\|\Pi_l \mathbf{Z}_l\|_2^2}{\|\mathbf{Z}_l\|_2^2}, \text{ add } m' \text{ to } \mathcal{A}.$$

Step 4 Let $\mathbf{X}_{\mathcal{A}} = (\cdots \mathbf{X}_j \cdots)_{j \in \mathcal{A}}$ and $\mathbf{X}_{\mathcal{A}}^T \mathbf{X}_{\mathcal{A}} = \mathbf{P} \Lambda \mathbf{P}^T$, where Λ and \mathbf{P} are the matrices of eigen values and eigen vectors of $\mathbf{X}_{\mathcal{A}}^T \mathbf{X}_{\mathcal{A}}$ respectively. Let $\tilde{\mathbf{X}}_{\mathcal{A}} = \mathbf{X}_{\mathcal{A}} \mathbf{P}$, $\alpha = \Lambda^{-1} \tilde{\mathbf{X}}_{\mathcal{A}}^T \mathbf{z}$ and $\sigma^2 = \frac{\mathbf{z}^T \mathbf{z} - \alpha^T \tilde{\mathbf{X}}_{\mathcal{A}}^T \mathbf{z}}{n - \#\mathcal{A} - 1}$. Compute $\beta_{\mathcal{A}} = \mathbf{P}(\mathbf{I} - \mathbf{K}(\Lambda + \mathbf{K})^{-1})\alpha$ where $\mathbf{K} = \text{diag}(k_1, \dots, k_{\#\mathcal{A}})$ and $k_i = \frac{2\sigma^2(n - \#\mathcal{A} - 1)}{\lambda_{\max} \alpha_i^2}$ for $i = 1, \dots, \#\mathcal{A}$ and λ_{\max} is the largest eigen value of $\mathbf{X}_{\mathcal{A}}^T \mathbf{X}_{\mathcal{A}}$.

Step 5 Assign the elements of β_{temp} corresponding to the selected variables by $\beta_{\mathcal{A}}$ and the rest equal to zero. Update the current regression coefficient vector $\beta_t = \beta_{t-1} + \beta_{temp}$, the current residual $\mathbf{z} = \mathbf{y} - \mathbf{X}\beta_t$ and the current design matrix $\mathbf{Z} = (\mathbf{I}_n - \Pi_{\mathcal{A}})\mathbf{X}$ where $\Pi_{\mathcal{A}} = \mathbf{X}_{\mathcal{A}}(\mathbf{X}_{\mathcal{A}}^T \mathbf{X}_{\mathcal{A}})^{-1} \mathbf{X}_{\mathcal{A}}^T$. Normalize \mathbf{Z} again.

Step 6 Update $t = t + 1$. Repeat Step 1 to Step 5 until the cardinality of \mathcal{A} reaches p .

In Step 1 variable having maximum absolute marginal correlation with the response is identified from the inactive set. In Step 2 the variables that are highly correlated with the variable identified in Step 1 are picked according to threshold

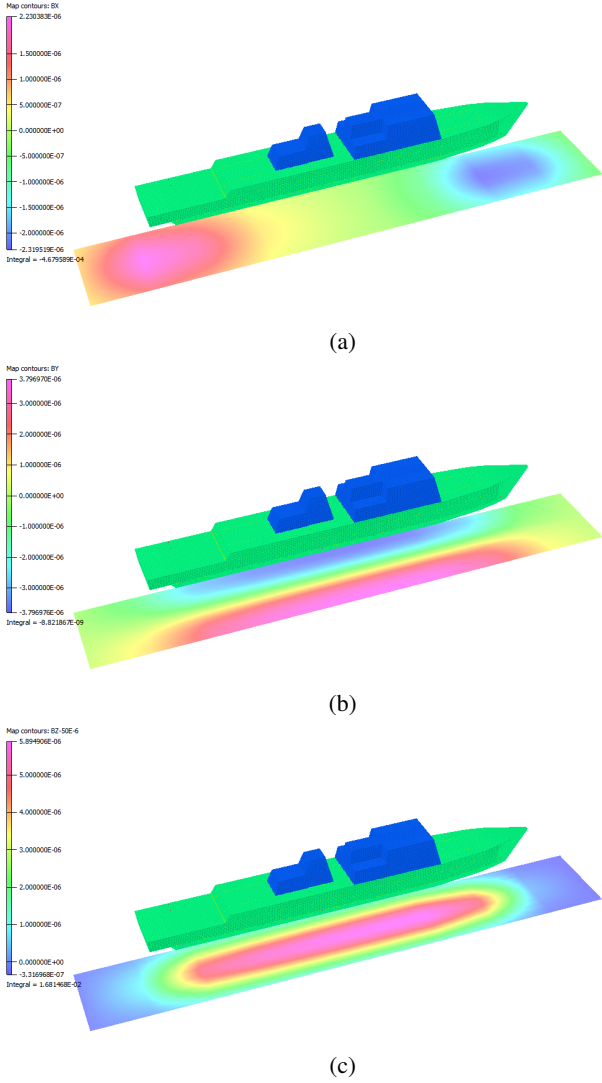


Fig. 10: Simulated DG OFF signature (tesla) for external inducing field $50 \mu T$ in the Z-direction. (a) X-component. (b) Y-component. (c) Z-component.

π_n . The threshold π_n in Step 2 is chosen as mentioned in [7], which changes at each iteration incorporating the correlation structure of the inactive set. In Step 3 the variable having maximum absolute tilted correlation with the response is included in the active set among those identified in Step 1 and Step 2. Tilted correlation quantifies the true association between the variable and the response by removing the impact of variables that are marginally correlated with the variable considered. In Step 4 ridge regression is performed on the active set and response. As the cardinality of \mathcal{A} reaches p , regression coefficients calculated from least squares will be erroneous. Thus, generalized ridge regression is used to regularize the regression coefficients through \mathbf{K} . The choice of ridge parameters \mathbf{K} in Step 4 is however subjective and one can tune them as per one's requirement based on the obtained results. The columns of matrix $\mathbf{X}_{\mathcal{A}}$ can be normalized if the variables do not have same units, and then $\beta_{\mathcal{A}}$ can be converted back to the original coefficients.

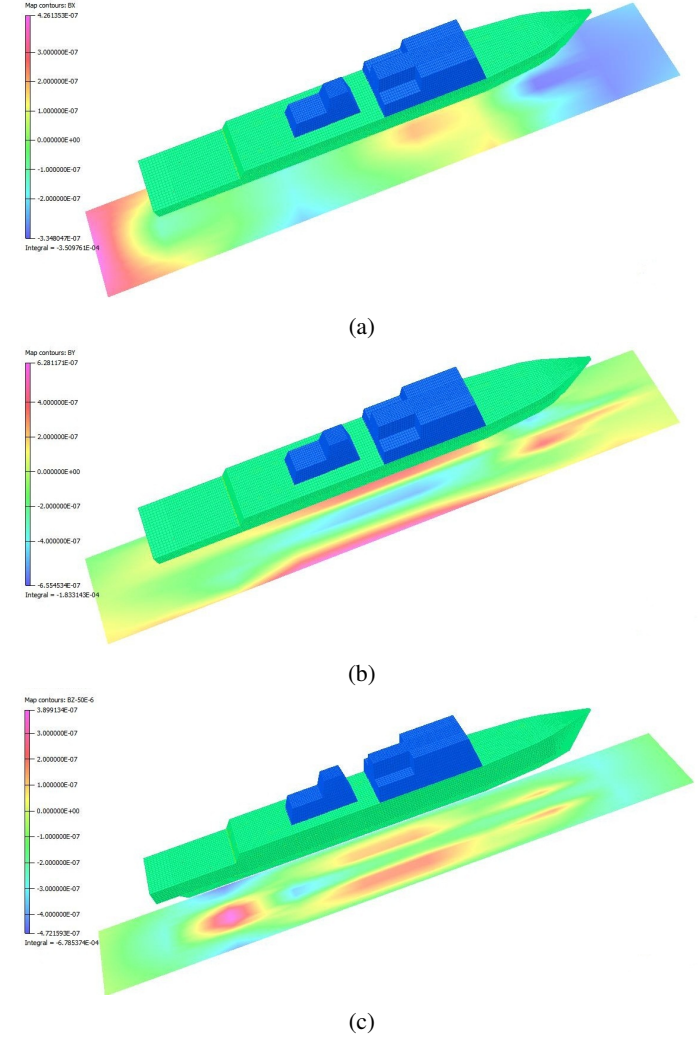


Fig. 11: Simulated DG ON signature (tesla) for external inducing field $50 \mu T$ in the Z-direction by applying coil currents obtained by TCS-GRR to the degaussing system. (a) X-component. (b) Y-component. (c) Z-component.

V. SIMULATIONS AND RESULTS

To illustrate the superiority of TCS-GRR over LARS we provide a detailed analysis of results by applying both of these model building algorithms to the test case when the external magnetic field is $50 \mu T$ in the Z-direction. Fig. 3 shows the reduction trend of the degaussing system “on” (DG ON) signature.

At each iteration, from the current residual response \mathbf{z} , observations for all the three directions have been extracted separately and the maximum of absolute values of corresponding components in the measurement grid is plotted against the number of steps as coils are added in the active set. It is clearly seen that there are large bumps in the signature reduction trend for LARS as compared to TCS-GRR. Also the DG ON signature finally crosses $2 \mu T$ mark in all the three directions when number of coils incorporated in the model are 22 and 17 for LARS and TCS-GRR respectively. Thus, the variables selected by TCS-GRR are more relevant than those selected by LARS, also the DG ON signature reduction obtained by TCS-GRR at the last iteration is nearly same as that for LARS.

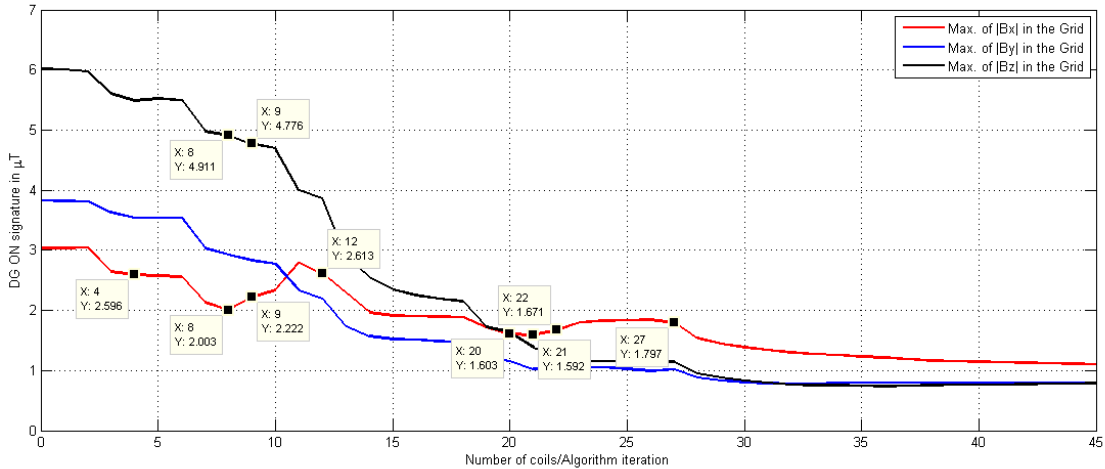


Fig. 12: Calculated DG ON signature reduction trend in the measurement grid for external field $50 \mu\text{T}$ in Z-direction by applying TCS-GRR.

Let the coils be assigned numbers as follows:

$$\begin{aligned} \{L3, L4, \dots, L16\} &\equiv \{1, \dots, 14\}, \\ \{A1p, A1s, A2p, \dots, A7s\} &\equiv \{15, \dots, 28\}, \\ \{M1d, M1u, \dots, M3, \dots, M8, M9d, M9u\} &\equiv \{29, \dots, 40\}. \end{aligned}$$

It is evident from Fig. 4 that the sequence of coils selected as the algorithm proceeds is indeed different for the two algorithms.

Fig. 5 and Fig. 6 show the currents assigned to the coils as the algorithms proceed. Fig. 7 shows the final coil currents, that is, negative of the regression coefficients, obtained at the last iteration of the algorithms. There are 28 coils for which the absolute value of coil currents obtained by TCS-GRR is comparatively less than that by LARS. Also since the regression coefficients obtained by both LARS and TCS proceed in least-squares estimate direction, at the final iteration for given set of variables we get the same regression coefficients. Thus, TCS-GRR which proceeds in the ridge estimate direction give regression coefficients, that have plausible magnitudes along with the same goodness of fit.

Fig. 8 shows the contour plots of the sampled magnetic signature, that is, DG OFF signature for the three components, whereas Fig. 9 shows the contour plots of the DG ON signature, that is, the residual response z obtained by TCS-GRR at the last iteration in the measurement grid. We have also labeled the respective maximum values of the signature components in the measurement grid. Fig. 10 shows the simulated magnetic signature on a Cartesian patch when the external inducing field of $50 \mu\text{T}$ is applied to the ship model whereas Fig. 11 shows the remnant magnetic signature after applying the coil currents obtained by TCS-GRR to the aforementioned 40 coils. We can see that the signature patterns in Fig. 9 and Fig. 11 are same, that is the calculated DG ON signature represent the simulated DG ON signature. Therefore, once we extract the individual coil effects and the sampled DG OFF signature data we can do analysis independent of the FEM software that requires large execution time. The above mentioned things are more clearly illustrated further by considering the design of coil L16.

We have applied the same procedure to different combinations of external inducing fields, Table I illustrates for various cases the maximum of absolute of DG OFF and DG ON signature components by applying TCS-GRR and LARS to the sampled data of signature and individual coil effects. Although for some cases we have exaggerated the external inducing fields, than that are practically been observed, still we can achieve significant magnetic signature reduction for all the three components in the measurement grid with the help of just 40 coils.

Now, consider all the coils mentioned in Fig. 2 except coils L1, L2 and L16. Thus we have total 45 coils. Here we will illustrate how we came up with coil L16. Fig. 12 shows the DG ON signature reduction trend for the above mentioned 45 coils. Fig. 13 shows the currents assigned to the coils as the algorithm proceed. Fig. 14 shows the calculated X-component of DG ON signature at different iterations of TCS-GRR in the measurement grid, whereas Fig. 15 shows the Z-component.

It is evident from Fig. 12 that the DG ON signature trend is monotonically decreasing for the Y- and Z-component, whereas for the X-component it is not the same case. We can prominently see two bumps in the graph of X-component. It is seen from Fig. 12 and Fig. 14(a-e) that the maximum value of the absolute of X-component in the measurement grid lies around the same region right from 4th iteration to 20th iteration. It is seen from Fig. 13(b) that coil M10d is included in the active set at the 9th iteration, due to which the Z-component of signature below the rear end of the ship is less than that at the 8th iteration as can be seen from Fig. 15. However, it is evident from Fig. 14(b-c) that the X-component of the signature below the rear end of the ship at the 9th iteration is more than at the 8th iteration, and it continues to increase until 12th iteration wherein coil L17 is included in the active set as can be seen from Fig. 12, Fig. 13(b) and Fig. 14(d). From 21st iteration onwards the maximum value of the absolute of X-component in the measurement grid occurs around the same region below the front end of the ship as can be seen from Fig. 12 and Fig. 14(f-h). Also it is seen from Fig. 13(c) that coil L18 is included in the active set at the 22nd iteration, due to which the X-component of signature around

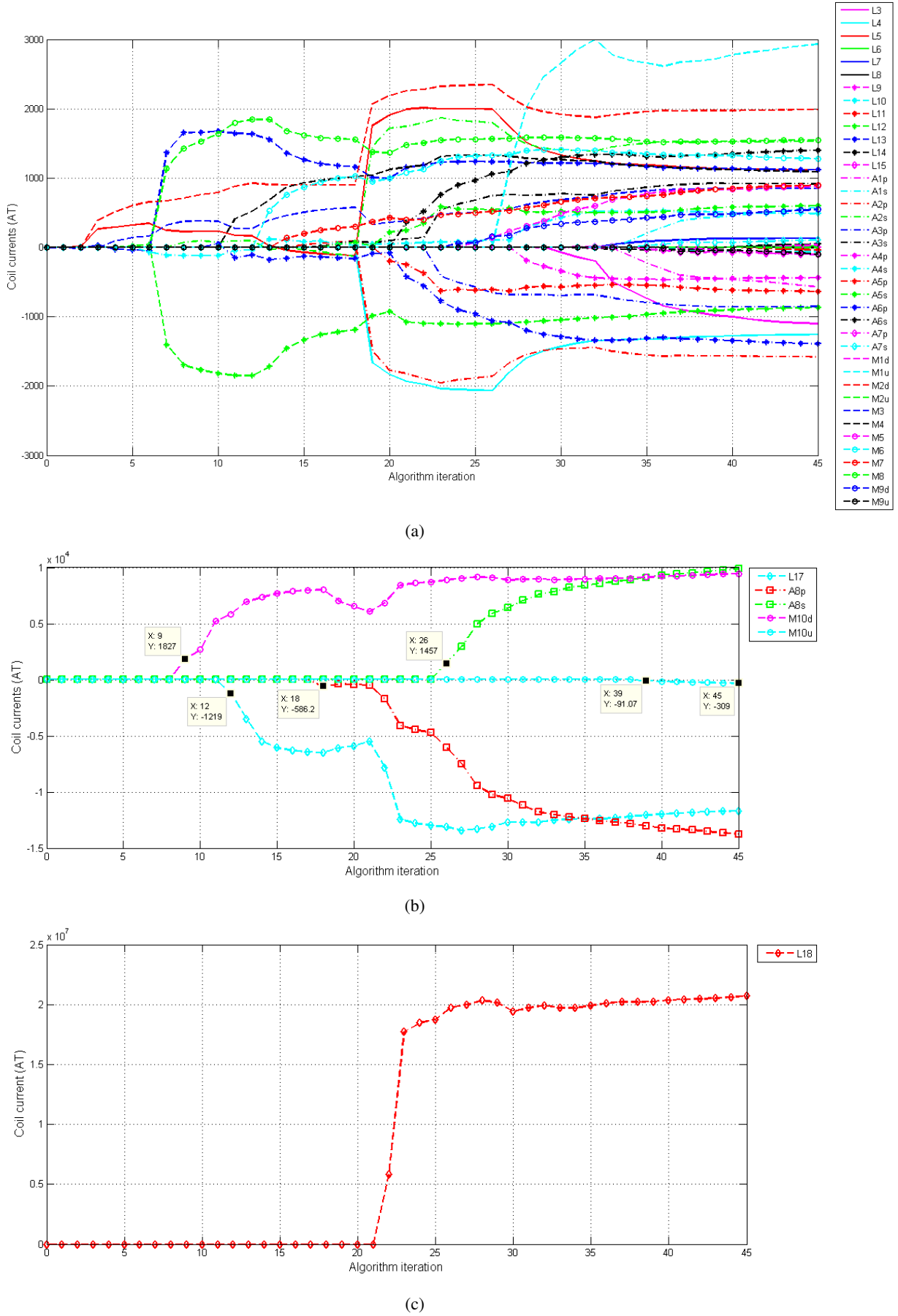


Fig. 13: The degaussing coil currents assigned by TCS-GRR for external field $50 \mu T$ in Z-direction.

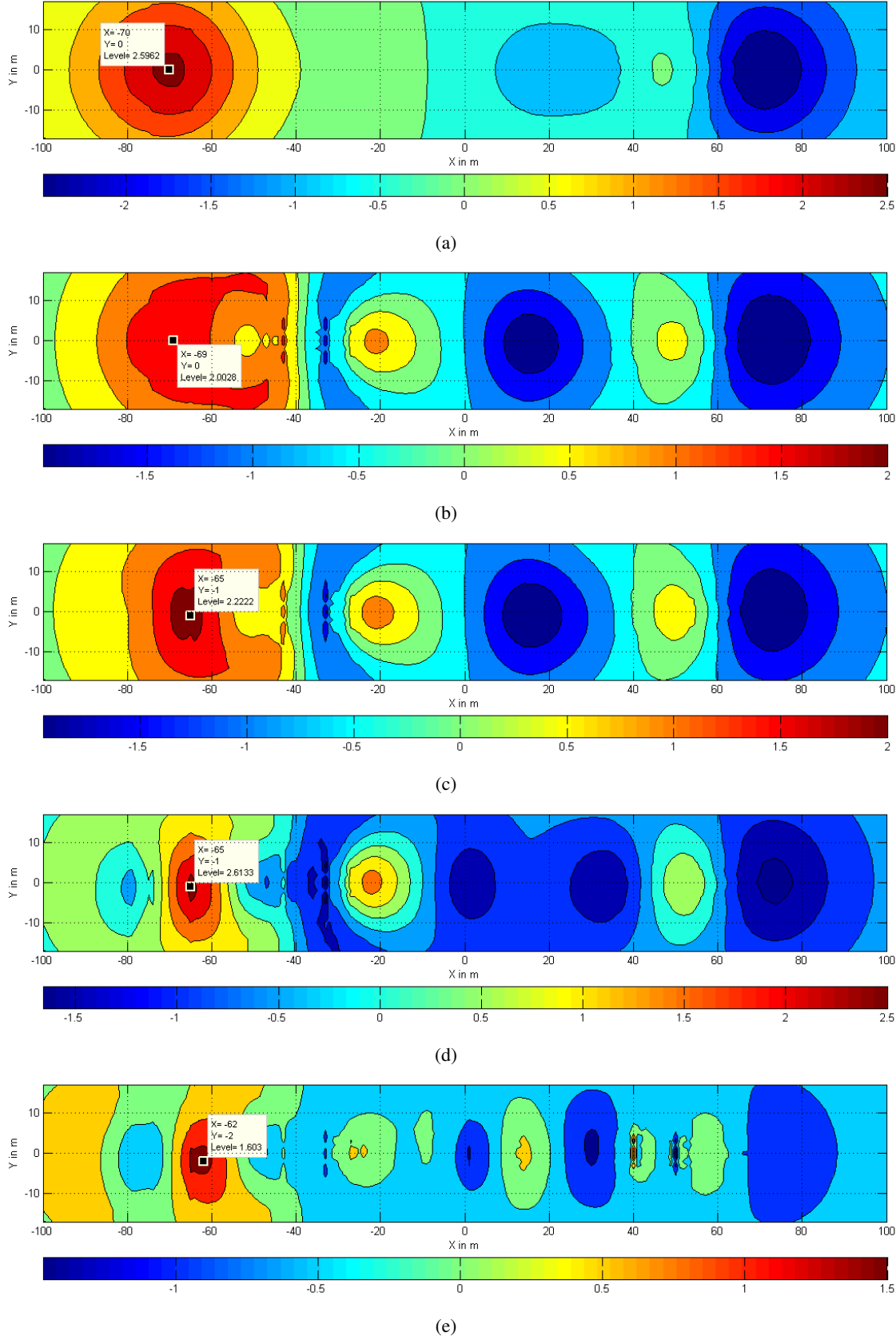


Fig. 14: Calculated X-component of DG ON signature (μT) at different iterations for external inducing field $50 \mu T$ in the Z-direction in the measurement grid. (a) Iteration 4. (b) Iteration 8. (c) Iteration 9. (d) Iteration 12. (e) Iteration 20.

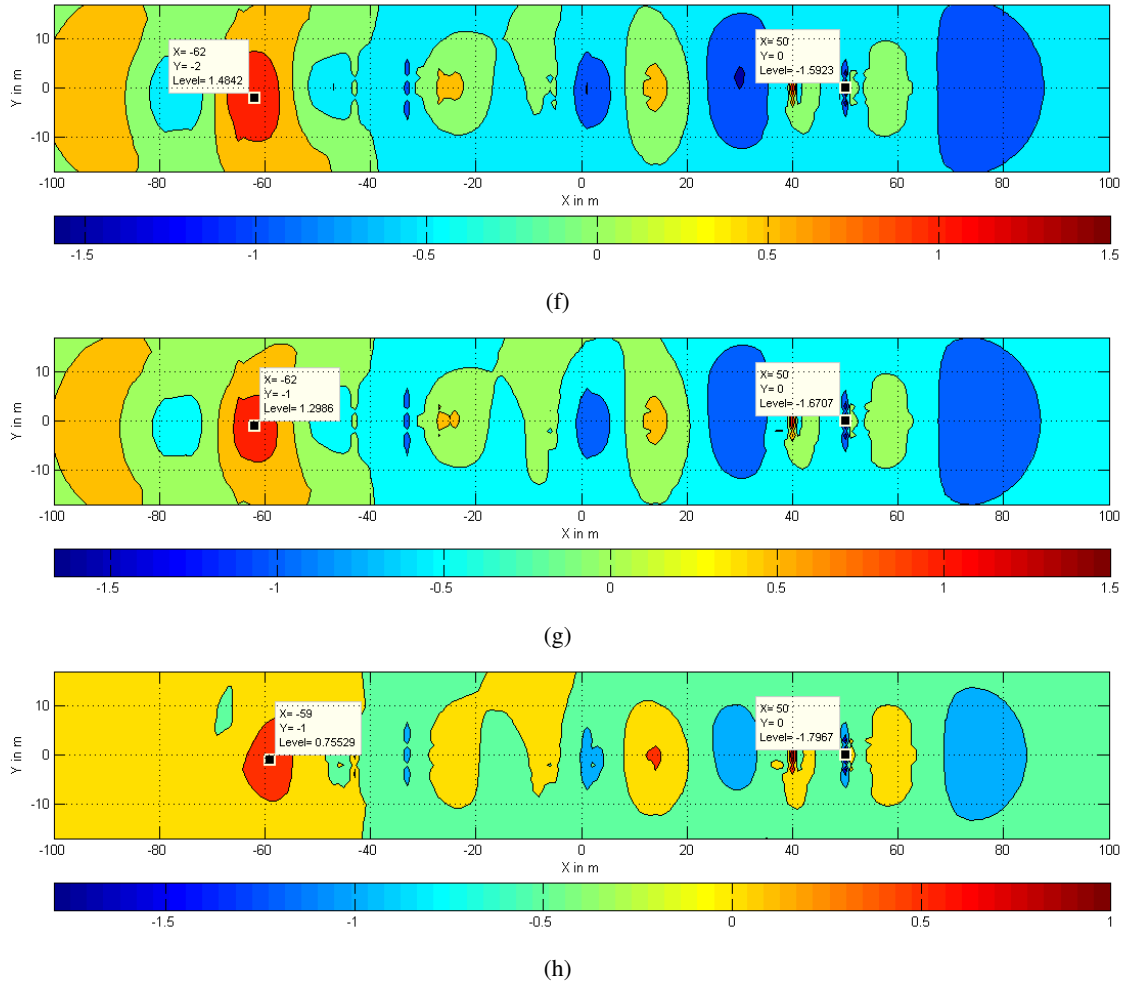


Fig. 14: (Continued.) Calculated X-component of DG ON signature (μT) at different iterations for external inducing field $50 \mu T$ in the Z-direction in the measurement grid. (f) Iteration 21. (g) Iteration 22. (h) Iteration 27.

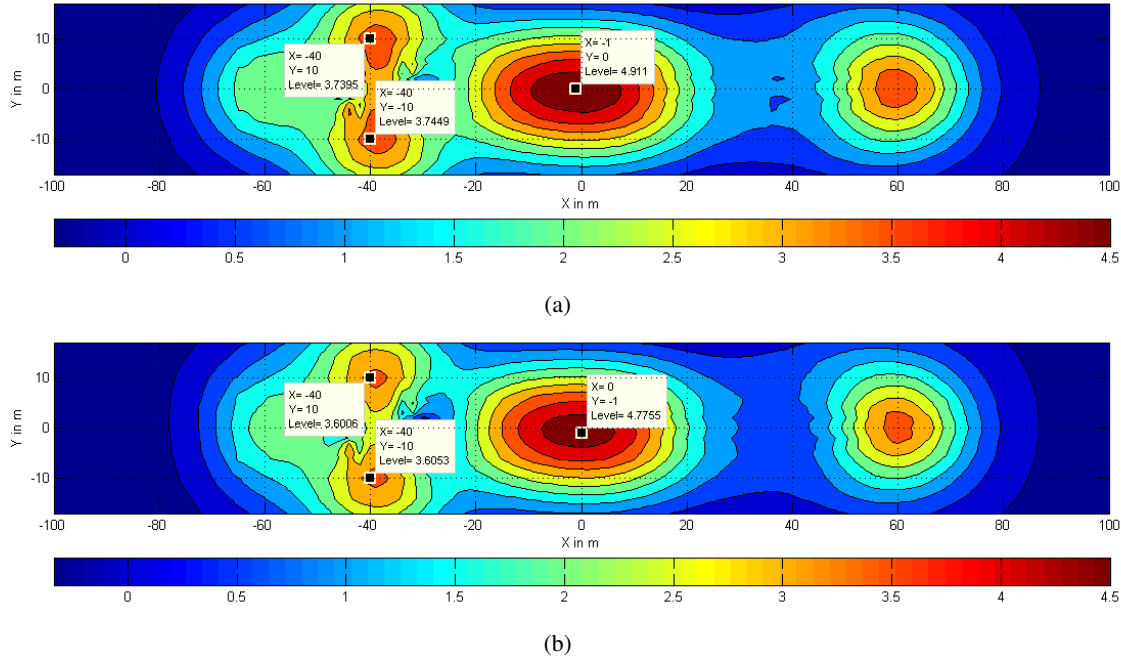


Fig. 15: Calculated Z-component of DG ON signature (μT) at different iterations for external inducing field $50 \mu T$ in the Z-direction in the measurement grid. (a) Iteration 8. (b) Iteration 9.

the region below the rear end of the ship further continues to decrease. Hence, from the above few lines we can say that inclusion of coil M10d does reduce the Z-component of the signature around the region below the rear end of the ship but worsens the X-component of the signature, leading to inclusion of coils L17 and L18. Also coil M10u like M10d is not that efficient. The placement of the coils L17 and L18 do not prove to be efficient as they require large currents, which is evident from Fig. 13(b-c). Thus, coil L16 due to its orientation and location, handles both X- and Z-component simultaneously. Also the maximum value of the absolute of X-component of signature below the front end of the ship start to reduce from 27th iteration when coil M1u is included in the active set as can be seen from Fig. 12 and Fig. 14(h). It is evident from Fig. 13(b) that coils A8p and A8s are assigned very large currents that are unrealizable and hence are omitted.

Thus, by analyzing the calculated DG ON signature reduction trend, currents assigned to the coils by the algorithm and the calculated DG ON signature patterns at different iterations we can address the problems associated with the existing or initial coils, by designing new coils or incorporating slight changes in the existing coils to get an optimal set of coils.

VI. CONCLUSION

The aforementioned 40 degaussing coils placed in the ship model are capable of reducing the signature by significant amounts for various combinations of external inducing fields. Keeping in mind the enormity of the ship, it is possible to further reduce the signature by placing more coils with providing better control on the signature. By using TCS-GRR we get to know the most relevant coils along with their estimated currents for signature reduction and also the insights for designing new coils. Thus, such techniques can be successfully implemented for designing an optimal degaussing system. Once such system is designed then the coils can be calibrated by applying regularized linear regression techniques that have faster execution time.

ACKNOWLEDGMENT

This work was supported by the Centre of Excellence (Complex and Non-linear Dynamical Systems), VJTI, Mumbai, India and TEQIP-II (subcomponent 1.2.1). The authors would like to thank V. Samala for technical assistance with COBHAM Opera3D throughout the course of research.

REFERENCES

- [1] J. J. Holmes, *Exploitation of a Ship's Magnetic Field Signatures*. San Rafael, CA, USA: Morgan & Claypool, 2006.
- [2] J. J. Holmes, *Reduction of a Ship's Magnetic Field Signatures*. San Rafael, CA, USA: Morgan & Claypool, 2008.
- [3] J. J. Holmes, "Application of models in the design of underwater electromagnetic signature reduction systems," *Naval Eng. J.*, vol. 119, no. 4, pp. 19-29, Nov. 2007, doi:10.1111/j.1559-3584.2007.00083.x.
- [4] D. J. Bekers and E. S. A. M. Lepelaars, "Degaussing system design optimization," in *Proc. 8th Int. Marine Electromagn. Conf.-MARELEC*, Hamburg, Germany, Jul. 2013, pp. 16-19.
- [5] B. Efron, T. Hastie, I. Johnstone, R. Tibshirani, "Least angle regression," *Ann. Statist.*, vol. 32, no. 2, pp. 407-499, 2004.
- [6] J. J. Holmes, S. Steffey, "Advanced degaussing coil system," US Patent 5483410, Jan. 9, 1996.
- [7] H. Cho, and P. Fryzlewicz, "High dimensional variable selection via tilting," *J. Roy. Statist. Soc. B*, vol. 74, no. 3, pp. 593-622, Jun. 2012.
- [8] Y. Benjamini and Y. Hochberg, "Controlling the false discovery rate: A practical and powerful approach to multiple testing," *J. Roy. Statist. Soc. B, (Methodol.)*, vol. 57, no. 1, pp. 289-300, 1995.
- [9] A. E. Hoerl and R. W. Kennard, "Ridge regression: Biased estimation for nonorthogonal problems," *Technometrics*, vol. 12, no. 1, pp. 55-67, Feb. 1970.
- [10] A.V. Dorugade, "New ridge parameters for ridge regression," *J. Assoc. Arab Univ. Basic and Appl. Sci.*, vol. 15, pp. 94-99, Apr. 2014.